ISSN 1063-7834, Physics of the Solid State, 2014, Vol. 56, No. 11, pp. 2185–2190. © Pleiades Publishing, Ltd., 2014.
Original Russian Text © A.D. Gorlov, 2014, published in Fizika Tverdogo Tela, 2014, Vol. 56, No. 11, pp. 2115–2120.

MAGNETISM

^{151,153}Eu Electron Paramagnetic Resonance in $SrMoO_4$ and Determination of Signs of Spin Hamiltonian Parameters at Different Temperatures

A. D. Gorlov

Research Institute of Physics and Applied Mathematics, Ural Federal University, pr. Lenina 51, Yekaterinburg, 620083 Russia

e-mail: Anatoliy.Gorlov@usu.ru

Received March 27, 2014; in final form, April 18, 2014

Abstract—The electron paramagnetic resonance (EPR) spectra of Eu^{2+} impurity centers in $SrMoO_4$ crystals have been studied in the temperature range of 1.8, 100–300 K. A hyperfine structure has been simulated for ^{151,153}Eu of different EPR transitions observed experimentally at different temperatures and external magnetic field orientations. A unique set of all parameters of the spin Hamiltonian for the known sign of the hyperfine interaction parameters A_i has been determined. It has been found that the diagonal parameters $|b_n^0|$ of the spin Hamiltonian decrease with increasing temperature; however, the parameter b_4^4 increases. The results of the study have demonstrated that $|b_2^0(T)/P_2^0(T)| \sim$ const for ^{151,153}Eu in this single crystal.

DOI: 10.1134/S1063783414110080

1. INTRODUCTION

Interest in the study of optical and electron paramagnetic resonance (EPR) spectra of crystals with the scheelite structure ($MeWO_4$, $MeMoO_4$) with a rare-earth metal (REM) impurity has not diminished, since it is associated with the development of new efficient materials for laser physics and acousto-optics [1]. Europium-doped molybdates are promising materials for applications in light-emitting diodes and thermography [2–5].

It is known [1] that the inhibition of relaxation processes with increasing ionic radius in the series Ca^{2+}, Sr^{2+}, Ba^{2+} and increasing lattice parameters, which is associated with the increase in the frequency of totally symmetric vibrations of the [WO_4, MoO_4] group, leads to Raman scattering line narrowing. These effects are directly related to steady contributions to REM ground state splitting and dynamic processes near impurity centers.

The spin Hamiltonian (SH) constants, which describe the EPR spectrum of impurity centers, are related to both lattice site coordinates and frequencies of vibrations whose amplitude depends on the lattice temperature [6–8]. Hence, the experimental dependences $b_n^m(T)$ of the parameters of the initial splitting of the impurity ground state and the constants describing the hyperfine structure (HFS) of EPR signals provide information about this relation and can be reference data for testing theoretical models of dynamic and static interactions near REM. The objective of the present work was the study in this direction.

The choice of Eu^{2+} impurity centers in $SrMoO_4$ single crystals (with a natural content of odd isotopes ^{151,153}Eu) is caused by the fact that the EPR spectrum of this ion in the *S*-state is observed in a wide temperature range, and the existence of appreciable quadrupole moments of the isotopes makes it possible to obtain the additional dependence $P_2^0(T)$ (the quadrupole interaction parameter determined by the crystal field gradient on the impurity). Similar studies for other ions in the *S*-state (Mn^{2+} and Gd^{3+}) in scheelite structures are well presented in the literature. However, there is only one work [6] dealing with the study of the temperature dependence of the parameters $b_n^m(T)$ for odd isotopes Eu^{2+} in $CaWO_4$. The results of [6] indicated a significant change in $b_2^0(T)$ up to a sign change, which is undoubtedly associated with the temperature dependence of the lattice parameters and phonon spectrum. There are still no reasonable estimates of temperature dependences of SH parameters for Eu^{2+} in $CaWO_4$. In our opinion, new experimental data for Eu^{2+} in isostructural crystals are necessary for deeper insight into the mechanisms resulting in temperature-related changes in the impurity energy structure.

Spin Hamiltonian parameters for $SrMoO_4 : Eu^{2+}$ (in MHz)

T, K	1.8	100	147	200	250	300
$g_\parallel$	1.991(1)	1.9913(5)	1.9915(7)	1.9914(5)	1.9914(5)	1.9912(5)
$g_\perp$	1.990(1)	1.9907(5)	1.9906(6)	1.9905(5)	1.9905(6)	1.9904(8)
b_2^0	814(2)	813.8(5)	813.1(4)	810.2(5)	807.0(5)	804.2(4)
b_4^0	−23.5(8)	−23.0(2)	−22.6(3)	−21.8(3)	−21.2(2)	−20.8(4)
b_6^0	0.65(35)	0.6(1)	0.6(2)	0.6(3)	0.6(2)	0.6(2)
b_4^4	64(8)	67.5(8)	70.0(7)	72.5(8)	74.3(8)	77.1(7)
			^{151}Eu			
$A_\parallel$	−102.3(9)	−102.2(4)	−102.0(4)	−101.7(4)	−101.6(5)	−101.6(5)
$A_\perp$	−102.2(9)	−101.5(4)	−100.9(4)	−101.0(4)	−100.9(5)	−100.9(5)
P_2^0	−10.9(6)	−10.7(4)	−10.7(4)	−10.7(4)	−10.7(5)	−10.7(5)
$\lvert b_2^0/P_2\rvert$	75(5)	76.2(30)	76.4(27)	75.8(29)	75.6(36)	75.3(34)
			^{153}Eu			
$A_\parallel$	−45(2)	−45.4(4)	−45.2(4)	−45.1(4)	45.0(4)	−45.0(4)
$A_\perp$	−45(2)	−45.0(4)	−44.9(4)	−45.0(4)	−45.0(4)	−44.9(4)
P_2^0	−27.8(9)	−27.8(4)	−27.8(4)	−27.7(4)	−27.7(5)	−27.6(5)
$\lvert b_2^0/P_2\rvert$	29.3(10)	29.3(4)	29.2(5)	29.2(4)	29.1(5)	29.1(5)

b_6^4, $b_6^6 \sim 0(2)$ at all temperatures, g_n are the tabulated values.

In methodical aspects, it is rather difficult to obtain reliable data on the parameters b_n^m from $^{151,153}Eu$ spectra of the crystals where REM is located in sites with local symmetry below cubic. The superposition of resonant signals simultaneously from two isotopes Eu^{2+} (electron spin $S = 7/2$, nuclear spin $I = 5/2$) with different parameters of hyperfine (HFI) A_i and quadrupole interactions complicates the HFS. Incorrect identification of observed structure components causes errors in the determination of HFI parameters A_i (an example is the study [9], where $A_\perp$ is overestimated for $^{151,153}Eu$ in $PbWO_4$). With this in mind, we present HFSs of some $^{151,153}Eu$ EPR transitions in $SrMoO_4$ for different orientations of the external magnetic field **H**. In [7, 8], the expressions are presented for the magnetic fields H_{res} for the HFS components determined using the perturbation theory to the second-order additions for $S = 1/2$, which make it possible to determine relative signs of the spin Hamiltonian parameters. However, as noted in [6], the description of both the Eu^{2+} EPR spectra of $CaWO_4$ and HFS signals using the perturbation theory (to the second order) is too inaccurate (for the crystal under study, the deviations are $\Delta H \sim 3$–15 G in the units of H_{res}). The simulation of experimental HFSs for EPR transitions in different **H** orientations, we described in [10], is based on numerical diagonalization of the energy matrix (48th order for $^{151,153}Eu$). This makes it possible to fairly simply determine the values and relative signs of all parameters necessary to describe the experimental EPR spectrum for spins $S > 1/2$ and $I > 1/2$ at any temperature. This method is well applicable to impurity centers located in sites with local symmetry below cubic, where the parameter P_2^0 defined by the crystal field gradient has a significant effect on the HFS of EPR signals.

The parameters b_n^m of this crystal at $T = 300$ K are given in [11]. They coincide with the data listed in the table. The results of [11] are in part presented in [12].

2. EXPERIMENTAL RESULTS AND DISCUSSION

The temperature studies of EPR spectra in different **H** orientations were performed using a Bruker EMX plus spectrometer in the 3-cm region. The first derivatives of EPR signals were recorded and then were numerically differentiated. The second derivatives $Y''(H)$ of signals obtained in such a way are shown

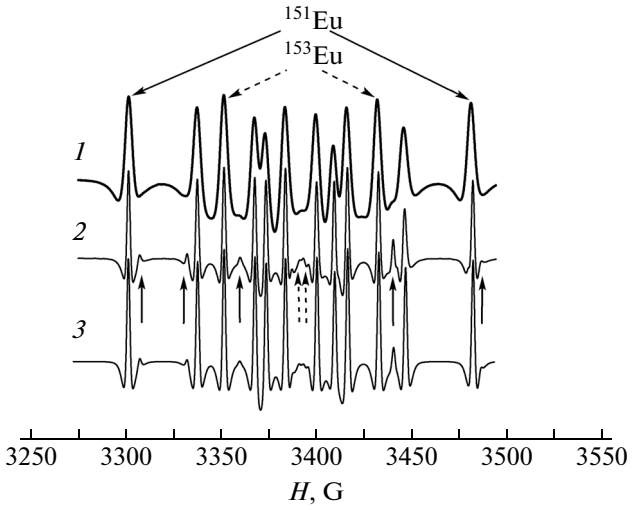

Fig. 1. Experimental HFSs at temperatures T = (*1*) 300 and (*2*) 100 K for the $|1/2, m_1\rangle \longleftrightarrow |-1/2, m_2\rangle$ transition ($Y''(H)$ at $\Theta = 0$, $\varphi = 0$). Solid (for ^{151}Eu) and dashed (for ^{153}Eu) arrows from below indicate forbidden transitions with $|\Delta m| = 1$, resulting from the small spread of S_4 axis directions in the crystal. (*3*) Simulated structure (T = 100 K) at $A < 0$, $P < 0$ and $\Theta = 0.8°$, $\varphi = 0$.

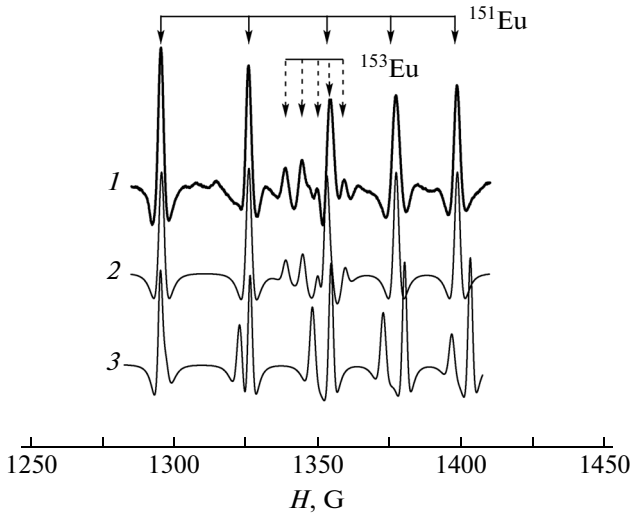

Fig. 2. Hyperfine structure of the forbidden $|-0.63, m_1\rangle \longleftrightarrow |1.49, m_2\rangle$ transition ($Y''(H)$ at $\Theta = 0$, $\varphi = 0$): (*1*) experiment, (*2*) simulated structure at $A < 0$, $P < 0$, and (*3*) simulated structure at $A < 0$, $P > 0$ (T = 100 K).

in all figures of the paper. The studied crystals were grown by the Czochralski method with a 0.1 wt % EuO impurity in the mixture.

The experimental Eu^{2+} EPR spectra of $SrMoO_4$ in different **H** orientations exhibit tetragonal local symmetry of the impurity center, which indicates its localization at the Sr^{2+} site in the crystal. Although the local symmetry of the Sr^{2+} site is S_4, the EPR spectra are well described by the spin Hamiltonian for higher symmetry D_{2d}, which was previously indicated in [6, 10, 11]. The coordinate system with $\mathbf{Z} \parallel \mathbf{S}_4$, i.e., the principal axis of the crystal symmetry was used. The **X** and **Y** directions in the perpendicular plane were defined by extrema of the angular dependence of EPR transitions (the high-field signal minimum in the *xy* plane corresponds to the **X** axis). The HFI tensor can be presented as the diagonal one with parameters $A_z = A_\parallel$ and $A_x = A_y = A_\perp$, and the quadrupole interaction is defined by the single parameter P_2^0 [7, 8],

$$H = 1/3 b_2^0 O_2^0 + 1/60(b_4^0 O_4^0 + b_4^4 O_4^4) + 1/1260(b_6^0 O_6^0 + b_6^4 O_6^4 + b_6^6 O_6^6) + g\beta(\mathbf{HS}) + \mathbf{SAI} + 1/3 P_2^0 O_2^0(I) - g_n\beta_n(\mathbf{HI}). \quad (1)$$

All notations in Eq. (1) are conventional [7, 8].

The parameters b_n^m, which describe the EPR spectra of odd Eu^{2+} isotopes at any temperature, were determined by numerical minimization of the root-mean-square deviations of experimental and calculated "centroids" of the HFS signals. The **H** directions were defined by angles Θ and φ ($\mathbf{H} \parallel \mathbf{Z}$ corresponds to $\Theta = 0$, $\varphi = 0$, $\mathbf{H} \perp \mathbf{Z} - \Theta = 90°$, $\varphi = 0, 45°$).

The constants $A_\parallel$, $A_x = A_y = A_\perp$ and P_2^0 (hereafter, $P_2^0 = P$ and $A = A_\parallel \approx A_\perp$) of odd isotopes were determined as in [10]. The difference between the experimental and calculated HFS positions is ≤1.5 G; for relative ones, it is ten times higher.

In the Eu^{2+} EPR spectra of $SrMoO_4$ in different **H** orientations, both intense allowed transitions $|M_1 m_1\rangle \longleftrightarrow |M_2 m_2\rangle$ with $\Delta M = M_1 - M_2 \approx -1$, $\Delta m = m_1 - m_2 \approx 0$ and weak forbidden ones with $|\Delta M| \geq 1$, $|\Delta m| \approx 1, 2$ are observed (see Figs. 1–4). Here, M_i are projections of the electron spin and m_i are projections of the nuclear spin, which characterize the energy levels $E(M_i m_i)$, where $E(M_1 m_1) < E(M_2 m_2)$. The most intense forbidden transitions are observed in the region of low magnetic fields at any **H** direction due to effective mixing of electron–nuclear states, which depends on the off-diagonal terms of the spin Hamiltonian. The quadrupole interaction almost has no effect on the probability at $\mathbf{H} \parallel \mathbf{Z}$, since it enters diagonal terms of the energy matrix. In other orientations, it is significantly involved in mixing of nuclear states [7, 8] within the multiplet M, where $\Delta E = E(Mm_1) - E(Mm_2) \sim A$ (at $A > P$). All these factors lead to a significant increase in the probability of transitions with $|\Delta m| \approx 1, 2$. In this case, their positions become asymmetric with respect to the HFS center and depend on the P sign.

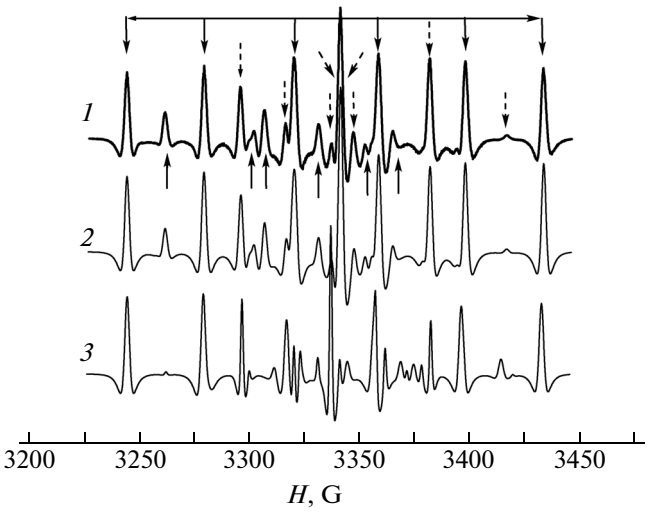

Fig. 3. (*1*) Hyperfine structure of the $|1/2, m_1\rangle \longleftrightarrow |-1/2, m_2\rangle$ transition ($\Theta = 90°$, $\varphi = 0$) at $T = 100$ K. Solid arrows from above and from below indicate the transitions for ^{151}Eu with $\Delta m \approx 0$ and $|\Delta m| = 2$, respectively. Dashed arrows from above indicate the transitions for ^{153}Eu with $|\Delta m| \approx 0, 1, 2, 3$. Simulated HFSs at (*2*) $A < 0$, $P < 0$, $b_2^0 > 0$ and (*3*) $A < 0$, $P > 0$, $b_2^0 > 0$.

2.1. $\mathbf{H} \parallel \mathbf{Z}$

In this orientation, the most resolved HFS is observed (components with half-widths from 2.3–10 G ($T = 100$ K) and 4–12 G ($T = 300$ K)) at different transitions. Changes in the ^{151,153}Eu EPR spectra with decreasing temperature consisted of changes in the positions of HFS signal centers, small decreases in the HFS component half-widths, and an increase in the splitting $\Delta H_{\max}$ (~1 G) between edge components of the HFS of one transition for all allowed transitions (see Fig. 1). For different forbidden transitions with $|\Delta M| > 1$ and $|\Delta m| \approx 1, 2$, $\Delta H_{\max}(T)$ for ^{151}Eu both increased and decreased. Such a difference in the $\Delta H_{\max}$ behavior for these transitions is due to the fact that the positions of HFS components are defined by both the diagonal and off-diagonal SH terms, and the competition between temperature-related changes of these contributions can lead to different dependences $\Delta H_{\max}(T)$, especially in the region where energy levels are close to each other or are "crossed."

It is simple to determine the value and sign of P (the sign of A is known) from the observation of any transition with $|\Delta m| > 0$, since there is a direct contribution of this parameter to both $\Delta H_{\max}$ and ΔH of neighboring HFS components. Using only the diagonal terms of the energy matrix obtained from Eq. (1), for $|M_1 m_1\rangle \longleftrightarrow |M_2 m_2\rangle$ and $|\Delta m| > 0$ we have

$$\Delta H_{\max} = |A + 2P\Delta m/\Delta M|(2I - |\Delta m|)/g\beta, \qquad (2)$$

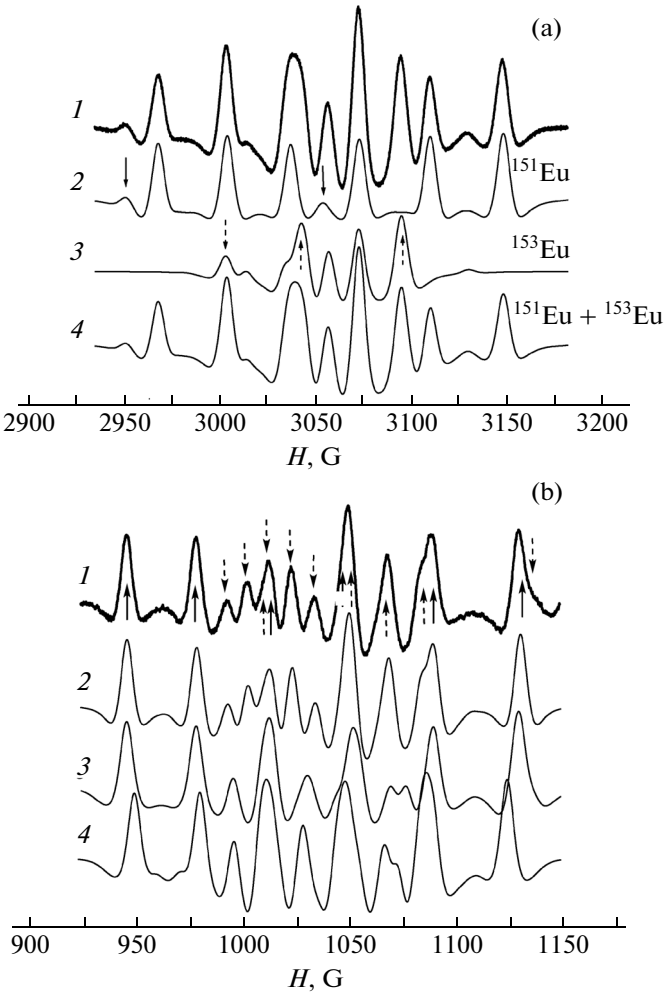

Fig. 4. (a) (*1*) Observed and (*2–4*) simulated HFSs of the $|-3/2, m_1\rangle \longleftrightarrow |-1/2, m_2\rangle$ transition ($Y''(H)$ at $\Theta = 90°$, $\varphi = 0$, $T = 300$ K). Solid arrows from above near curve *2* for ^{151}Eu indicate forbidden transitions ($|\Delta m| \approx 2$), dashed arrows near curve *3* indicate allowed transitions ($\Delta m \approx 0$) for ^{153}Eu; and curve *4* shows the total structure at $A < 0$, $P < 0$, $b_2^0 > 0$. (b) (*1*) Experimental HFS of the $|-1.23, m_1\rangle \longleftrightarrow |1.92, m_2\rangle$ transition with $|\Delta m| \sim 0, 1, 2$ ($\Theta = 90°$, $\varphi = 0$, $T = 100$ K) and simulated structures at (*2*) $A < 0$, $P < 0$, $b_2^0 > 0$, (*3*) $A < 0$, $P > 0$, $b_2^0 > 0$, (*4*) $A < 0$, $P < 0$, $b_2^0 < 0$. Solid and dashed arrows from below indicate transitions for ^{151}Eu and ^{153}Eu, respectively ($\Delta m \sim 0$). Dashed arrows from above indicate the most intense forbidden transitions for ^{153}Eu ($|\Delta m| \sim 1, 2$).

where $2I - |\Delta m|$ is the number of intervals between components (here, $|\Delta m|$ is an integer).

Then, if $\Delta H_{\max} > |A|(2I - |\Delta m|)/g\beta$ (for $\Delta M < 0$, $\Delta m > 0$, and $|A| > |P|$), then A and P signs are opposite, and vice versa. This criterion is well satisfied for ^{153}Eu ($P \approx 0.5$ A), but is poorly fulfilled for ^{151}Eu due to a significant contribution of nondiagonal terms of the spin

Hamiltonian to H_{res} in comparison with the contribution of $P \approx 0.1$ A. In the case of $|P| > |A|$, when ΔH is defined by P, at opposite-sign A and P, the condition $\Delta H_{max} > 2P\Delta m(2I - |\Delta m|)/\Delta M g\beta$ is satisfied (for $\Delta M < 0$, $\Delta m > 0$). For example, this is valid for ^{157}Gd in $PbMoO_4$, where forbidden transitions at $\mathbf{H} \parallel \mathbf{Z}$ are also observed (see [10, Fig. 3]).

Figure 2 shows the experimental record of the forbidden transition ($\Delta M \approx -2$, $\Delta m \approx 1$), where HFS components for two Eu^{2+} isotopes and simulated structures are quite well resolved. We can see that the best agreement is observed at $P_2^0 < 0$ if $A_\parallel < 0$, which is confirmed by HFS simulation for other forbidden transitions (see [12, Fig. 1]).

If we refer to the experimentally observed HFS of the $1/2 \longleftrightarrow -1/2$ transition at $T = 100$ K (Fig. 1), it can be noted that weak signals are observed near intense components. These are also forbidden transitions with $\Delta M \approx -1$ and $|\Delta m| \approx 1$, shown in Fig. 1 by arrows from below. According to calculations in the orientation $\Theta = 0$, $\varphi = 0$, their probability is zero. In the experiments, it was impossible to achieve their disappearance; therefore, we assumed that their appearance is associated with the crystal imperfection, i.e., with the spread of S_4 axis directions in the crystal bulk. The HFS simulation at $\Theta > 0$, $\varphi = 0$, and $P < 0$ (here ΔM is identical for allowed and forbidden transitions) for this signal showed that the possible spread is $\Delta\Theta \geq 0.8°$, and variations $\Delta\varphi \approx 2°$ have a weak effect on the structure. The structure simulation at $P > 0$ showed that the strongest forbidden transition should coincide with the first (in field) intense component, which contradicts the experimental HFS. Thus, the study of the HFS shape in the $\mathbf{H} \parallel \mathbf{Z}$ orientation showed that $P < 0$.

2.2. $\mathbf{H} \perp \mathbf{Z}$ ($\Theta = 90$, $\varphi = 0$)

In this orientation, the half-widths of HFS components for two Eu^{2+} isotopes are 3.5–19 G ($T = 100$ K) and 5–20 G ($T = 300$ K) at different EPR transitions and, almost at all transitions, HFS components are overlapped. An analysis of the observed intense transitions shows that the HFS is a superposition of both allowed ($\Delta M \approx -1$, $\Delta m \approx 0$) and forbidden transitions ($\Delta M \approx -1$, $|\Delta m| \approx 1, 2$) with close intensities. Figure 3 shows the EPR transition $1/2 \longleftrightarrow -1/2$ with the best resolution of HFS components. Solid arrows from above show field-edge intense transitions (^{151}Eu) with $\Delta m \approx 0$. Solid arrows from below show forbidden transitions with $|\Delta m| \approx 2$, whose amplitudes are only three times smaller than that of allowed ones. For ^{151}Eu, all intense components are transitions with $\Delta M \approx -1$, $\Delta m \approx 0$, whereas intense signals for ^{153}Eu are transitions with $\Delta M \approx -1$, $|\Delta m| \approx 0, 1, 2, 3$ (dashed arrows). The strongest signal at the HFS center is caused by three merged transitions with $\Delta m \approx -1$, while less intense signals are transitions with $|\Delta m| \approx 2$. As an example, Fig. 4a shows the experimental HFS (curve *1*) of the $-3/2 \longleftrightarrow -1/2$ transition, where HFSs were separately simulated (curves *2*, *3*) for two Eu^{2+} isotopes. The HFS of ^{151}Eu represents six intense transitions ($\Delta m \approx 0$) and two observed forbidden transitions $|\Delta m| \approx 2$ (arrows from above in Fig. 4a (curve *2*)). Dashed arrows in Fig. 4a (curve *3*) indicate allowed transitions for ^{153}Eu. Calculations show that the intense low-field component in Fig. 4a (curve *3*) is the superposition of the transitions $\Delta M \approx -1$, $\Delta m \approx 0$ and $\Delta M \approx -1$, $\Delta m \approx -1$, and the high-field component is a single transition with $\Delta M \approx -1$, $\Delta m \approx 0$. Only for transitions such as $|5/2| \longleftrightarrow |7/2|$, all intense HFS components can be attributed to allowed transitions, since the degree of nuclear state mixing due to the quadrupole interaction is lower in this case because of large splitting of nuclear sublevels ($\sim M_i A$, where $M_i = 5/2$, $7/2$). However, the experimental width of these signals is such that only edge HFS components belonging to ^{151}Eu are separately observed. Therefore, in our opinion, $A_\perp$ for experimental observed structures can be simpler estimated by simulation, as shown in Figs. 3 and 4.

Figure 4b shows the experimental and simulated HFSs of the $|-1, 24, m_1\rangle \longleftrightarrow |1.93, m_2\rangle$ transition. Solid arrows from below are transitions with $\Delta m \approx 0$ (^{151}Eu), dashed arrows are transitions with $|\Delta m| \approx 0, 1, 2$ (^{153}Eu). The simulated HFSs in Figs. 3 and 4 point to the dependence of their shape on relative signs of b_n^m and P, and the HFS for ^{153}Eu changes most critically. The dependence of the HFS shape on relative signs of b_2^0 and P is described in [10], but for the case where $P > A_i$.

Hence, we can argue that the table lists the unique set of values (within experimental error) of the parameters of the spin Hamiltonian at which the experimental and simulated structures are identical for all studied magnetic field orientations.

An analysis of the data presented in the table shows that the maximum temperature-related change $\Delta b_2^0 = [b_2^0(1.8\text{ K}) - b_2^0(300\text{ K}) \times 100/b_2^0(100\text{ K}) \sim 1.2\%$ and $|b_2^0/P_2^0| \approx$ const within experimental error for this crystal. A similar relation is satisfied for Gd^{3+} in $PbMoO_4$, YVO_4 [10], $SrMoO_4$ (preliminary results), and $CaWO_4$ [13]; however, judging by the results [6], it is violated for Eu^{2+} in $CaWO_4$. For comparison, Δb_2^0 for Gd^{3+} in $CaWO_4$, $CaMoO_4$, $SrMoO_4$, and $PbMoO_4$ is ~2%, ~2.6%, ~2.7%, and ~3.5%, respectively, as the temperature changes from 100 to 300 K.

The dependence $b_2^0(T)$ in the crystal under study is similar to those for Gd^{3+} in different crystals [10, 13, 14], but differs from that for Eu^{2+} in $CaWO_4$ [6]. In

[13], based on the Newman superposition model [15] with "intrinsic" parameters [16], the contribution $\Delta b_2^0(\text{lat})$ depending on temperature-related changes in lattice constants [17] was calculated for Gd^{3+} in $CaWO_4$. It was found that an increase in the temperature results in $\Delta b_2^0(\text{lat}) < 0$, hence, the phonon contribution $\Delta b_2^0(\text{phon}) > 0$. We performed a similar calculation for Eu^{2+} in $CaWO_4$ using the data of [6, 17] and obtained an identical result. In this case, the model parameter $b_{2p}(R_0)$ was taken from [11] and used to determine $b_{2s}(R_0)$ at $T = 5$ K. In our opinion, this parameter should be determined only at low temperatures, where $\Delta b_2^0(\text{phon})$ is small, since it is controlled by zero-point vibrations of the lattice [6–8, 14]. Then, $b_2^0(\text{exp})$ is completely defined by lattice parameters. Analogy would suggest that small temperature-related changes in $b_2^0(T)$ for Eu^{2+} in $SrMoO_4$ are associated with the strong compensation for changes in b_2^0 due to both lattice vibrations and expansion.

We did not analyze temperature-related changes in the parameter $b_4^m(T)$, since there is no adequate calculation model. It follows from the data presented in the table that the $|b_4^0(T)|$ variation decreases, which was previously observed [6, 10, 12, 14] for both Eu^{2+} and Gd^{3+} in isostructural crystals.

3. CONCLUSIONS

The simulation of the HFS allows us to understand what transitions form it and thus to avoid errors in the determination of HFI parameters and their signs. The weak temperature dependence of b_2^0 for the studied crystal is most likely caused by the compensation of the static (an increase in the lattice parameters with increasing temperature) and dynamic (due to a change in the amplitude and frequency of lattice site vibrations) contributions.

ACKNOWLEDGMENTS

This study was supported by the Ministry of Education and Science of the Russian Federation within the framework of the State Task Program (project code 2457) using equipment of the Joint Use Center "Modern Nanotechnologies" of the Ural Federal University.

REFERENCES

1. V. Osiko and I. Shcherbakov, Fotonika **39** (3), 14 (2013); T. T. Basiev, E. V. Zharikov, and V. V. Osiko, Crystallogr. Rep. **47** (1), 515 (2002).
2. Jie Liu, Hongzhou Lian, and Chunshan Shi, Opt. Mater. **29**, 1591 (2007).
3. J. Brübach, T. Kissel, M. Frotscher, M. Euler, B. Albert, and A. Dreizler, J. Lumin. **131**, 559 (2011).
4. Y. Shimodaira, H. Kato, H. Kobayashi, and A. Kudo, Bull. Chem. Soc. Jpn. **80**, 885 (2007).
5. A. A. Kaminskii, S. N. Bagaev, K. Ueda, K. Takaichi, and H. J. Eichler, Crystallogr. Rep. **47** (4), 653 (2002).
6. J. S. M. Harvey and H. Kiefte, Can. J. Phys. **47**, 1505 (1969).
7. W. Low, *Paramagnetic Resonance in Solids* (Academic, London, 1960; Inostrannaya Literatura, Moscow, 1962).
8. A. Abragam and B. Bleaney, *Electron Paramagnetic Resonance of Transition Ions* (Oxford University Press, Oxford, 1970; Mir, Moscow, 1972), Vol. 1.
9. T. H. Yeom, I. G. Kim, S. H. Lee, S. H. Choh, T. H. Kim, and J. H. Ro, J. Appl. Phys. **87**, 1424 (2000).
10. A. D. Gorlov, Phys. Solid State **55** (5), 960 (2013).
11. V. A. Vazhenin, A. D. Gorlov, L. I. Levin, K. M. Starichenko, S. A. Chikin, and K. M. Eriksonas, Sov. Phys. Solid State **29** (10), 1744 (1987).
12. A. D. Gorlov, in *Book of Abstracts of International Conference "Modern Development of Magnetic Resonance," Kazan, Russia, September 24–28, 2013*, p. 70.
13. A. D. Gorlov and I. N. Kurkin, in *Book of Abstracts of the XV International Feofilov Symposium on Spectroscopy of Crystals Doped with Rare-Earth and Transition Metal Ions, Kazan, Russia, September 16–20, 2013*, p. 172.
14. J. S. M. Harvey and H. Kiefte, Can. J. Phys. **49**, 995 (1971).
15. D. J. Newman and W. Urban, Adv. Phys. **24**, 793 (1975).
16. L. I. Levin and A. D. Gorlov, J. Phys.: Condens. Matter. **4**, 1981 (1992).
17. A. Senyshyn, M. Hoelzel, T. Hansen, L. Vasylechko, V. Mikhailik, H. Krausf, and H. Ehrenberg, J. Appl. Crystallogr. **44**, 319 (2011).

Translated by A. Kazantsev